Available online at www.sciencedirect.com

ScienceDirect

Procedia CIRP 124 (2024) 746–750

www.elsevier.com/locate/procedia

13th CIRP Conference on Photonic Technologies [LANE 2024], 15-19 September 2024, Fürth, Germany

Generating brick-like melt pools for Laser-Based Powder Bed Fusion using flexible beam shaping: a proof of concept on bead-on-plate single tracks

Jonas Grünewald[a,*], Robin Prudlik[a,b], Vijaya Holla[c], Philipp Kopp[d], Richard Off[a], Thomas Stoll[a], Stefan Kollmannsberger[d], Katrin Wudy[a]

[a]*Professorship of Laser-based Additive Manufacturing, TUM School of Engineering and Design, Technical University of Munich, Freisinger Landstraße 52, 85748 Garching, Germany*

[b]*Oerlikon AM Europe GmbH, Freisinger Landstraße 52, 85748 Garching, Germany*

[c]*Chair of Computational Modeling and Simulation, TUM School of Engineering and Design, Technical University of Munich, Arcisstraße 21, 80333 Munich, Germany*

[d]*Chair of Data Science in Civil Engineering, Bauhaus University Weimar, Coudraystraße 13A, 99423 Weimar, Germany*

* Corresponding author. Tel.: +49 89 289 55321. *E-mail address:* jonas.gruenewald@tum.de

Abstract

Despite the highest industrial maturity among additive manufacturing processes, laser-based powder bed fusion of metals (PBF-LB/M) lacks the productivity to further establish as an industrial manufacturing process. One approach for adjusting the melt pool shape to increase productivity in PBF-LB/M is spatial beam shaping. The freedom of beam shaping is almost unlimited, owing to modern optical concepts. The key is a beam shape optimized for a specific target. In this publication, the target is a brick-like melt pool cross-section. The publication demonstrates how the corresponding laser beam shape is designed using numerical optimization. The computed beam shape is reproduced using reflective spatial light phase modulators. The calculation is validated based on single-track experiments. Applying the optimized beam shape results in a melt pool shape similar to the optimization target. The width and depth of the melt track produced deviate by a maximum of 7 % from the specified target values.

Keywords: Additive Manufacturing; PBF-LB/M; LCOS-SLM; IN718; Beam Shape Optimization

1. Introduction

Laser-based powder bed fusion of metals (PBF-LB/M according to DIN EN ISO/ASTM 52900) is an additive manufacturing process in which metal components are fused layer-by-layer using a hatched laser exposure in a powder bed. In the state-of-the-art, single-mode fiber lasers with a Gaussian intensity profile are typically used as beam sources. Due to the diffraction-limited beam properties, very small spots are achieved, which are advantageous for creating small and filigree features in PBF-LB/M. Typically, spot sizes in the range of 30 – 115 µm are used [1]. However, the small spot sizes severely limit the productivity of the process. In typical industrial systems, build rates of up to 5 mm³/s are achieved during exposure [2]. Considering the scan speed v_{scan}, the hatch distance h, and the powder layer thickness t_{powder}, the build rate is calculated as

Nomenclature

h	Hatch distance
P_{laser}	Laser power
t_{powder}	Powder layer thickness
$\dot{V}$	Build rate
v_{scan}	Scan speed

2212-8271
10.1016/j.procir.2024.08.216

$$\dot{V} = v_{scan} \cdot h \cdot t_{powder}. \quad (1)$$

To increase this build rate, the powder layer thickness, the scanning speed, or the hatch distance must be increased. Increasing the powder layer thickness leads to a higher tendency of balling [3]. In addition, a higher layer thickness reduces the part resolution in the build direction. The scanning speed is typically optimized to a fluid mechanically stable maximum. If the scanning speed is increased further, fluid mechanical effects in the melt pool frequently cause humping and balling effects, which in turn pose a risk to process reliability [4]. The remaining parameter is the hatch distance. In order to increase the hatch distance and simultaneously produce dense components, wide melt pool cross-sections with a sufficient weld penetration depth are required. The approach presented in this paper aims to create melt pool cross-sections that are as rectangular as possible. These melt pools are to be assembled additively like bricks. The process is intended to be more efficient without multiple remelting of material.

The underlying approach is already being increasingly investigated in heat conduction welding and PBF-LB/M by using non-Gaussian beam profiles when processing different materials. When processing aluminum alloys (AlSi7Mg0.6 [5] AlMg4.5Mn0.7 [6], AlSi10Mg [7]), AISI 316L [8], CoCrMo [9, 10], and IN738LC [11], it has been shown that ring-shaped beam profiles produce shallower, wider melt pool cross sections. Also, a distortion of the spot by deformable mirrors [12] and diffraction-based beam splitting approaches [13, 14] result in wider shallow melt pools. The published studies focus on the process results for various predefined beam profiles. How the respective beam profile was designed is rarely published. In this study, this gap is filled by first optimizing a beam profile to a desired temperature distribution and secondly demonstrating the influence of the optimized beam shape on the process result by experimental validation using bare plate single-track experiments.

2. Materials and Methodology

The following sections describe the materials, system techniques, and methods for calculating an optimized beam shape, experimentally generating this beam shape, and conducting the corresponding process investigations.

2.1. Material

The precipitation-hardenable nickel-chromium alloy IN718 is used as the feedstock material. The material is prepared as 14 mm sheet metal and is sandblasted before the experiments to roughen the surface ($S_a \approx 0.5$ µm). No powder is applied during the experiments. Table 1 shows the chemical composition of the plates used. For the inverse calculation of the investigated beam shape, the thermophysical properties were assumed according to [15]. The approximations are listed in Table 2.

Table 1. Chemical composition of used IN718.

	Fe	Ni	Cr	Nb+Ta	Mo	Ti	Al	Co	Si	Mn
wt.%	Bal.	53.04	18.11	5.06	3.04	1.03	0.57	0.13	0.06	0.04

Table 2. Material and model parameters.

Density	8440 kg/m³
Specific heat capacity at 0 °C	425 J/kgK
Temperature derivative of specific heat capacity	$189.65 \cdot 10^{-3}$ J/kg
Heat conductivity at 0 °C	9.94 W/mK
Temperature derivative of heat conductivity	$13.9 \cdot 10^{-3}$ W/m
Latent heat of fusion	$2.8 \cdot 10^{5}$ J/kg
Solid temperature	1290 °C
Liquid temperature	1350 °C
Laser absorptivity	0.45

2.2. System technology

A commercial PBF-LB/M system (M300, EOS GmbH Electro Optical Systems, Krailling, Germany) with a modified beam guiding and shaping unit (patent pending by EOS GmbH Electro Optical Systems, Krailling, Germany) is used as a base machine. The beam is shaped using a liquid crystal on a silicon spatial light modulator (LCOS-SLM). With this optical system, the phase angles of the incident radiation can be shifted pixel-by-pixel. That way, a shaped wavefront is generated. In the Fourier plane of the optical system (processing plane), constructive and destructive interferences arise at various points due to the shaped wavefront. As a result, a variety of intensity distributions can be generated. The basic principle of the system is sketched in Fig. 1. The design of the phase masks is calculated based on an iterative Fourier transform algorithm (IFTA) using the Diffractive Optics Package of VirtualLab Fusion (LightTrans International GmbH, Jena, Germany).

2.3. Beam shape design

The laser beam shape optimization framework, presented in [16], is employed to design a beam shape for generating a brick-like melt pool cross-section. The first step towards the beam shape design is defining the desired melt pool shape and the resulting temperature distribution.

To provide the optimization algorithm with a physically achievable target temperature distribution, a steady-state thermal PBF-LB/M simulation is set up, where the standard laser heat source is replaced by a box-constraint of the temperature field to 2300 °C. This box constraint represents the desired melt pool shape and is 275 µm wide, 400 µm long, and 15 µm high. The velocity of the temperature constraint is

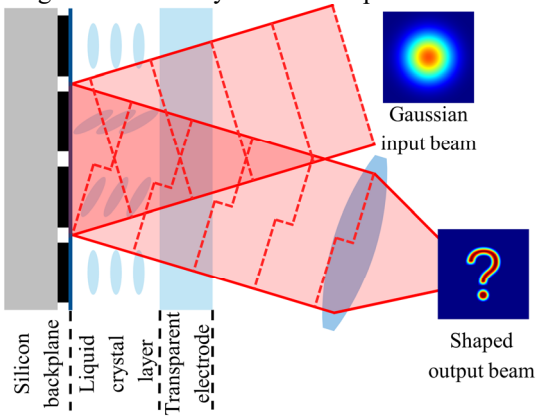

Fig. 1. Working principle of beam shaping with LCOS-SLM.

700 mm/s in the scan direction. The 2300 °C are significantly above the melting temperature of IN718 of 1290 °C, so the heat diffuses enough to yield a smooth melt pool surface. Fig. 2a shows the box constraint and the resulting melt pool as a contour surface at 1290 °C. The bounding box of this target melt pool is approximately 340 µm wide and 60 µm high. The resulting temperature distribution of this approach is shown in Fig. 2b. Only the temperature distribution outside the target melt pool is considered when calculating the beam shape. The grey area in Fig. 2b is not part of the target distribution, preventing any influence of the artificial temperature inside the melt pool and providing more freedom for the optimization.

Starting from an initial guess, the optimization algorithm [16] iteratively improves the beam shape to better approximate the target temperature distribution. After the optimization, the laser beam shape is post-processed to replace spurious negative intensities with zero. Fig. 2c and Fig. 2d show the final optimized temperature distribution and melt pool shape. The laser absorption coefficient is calibrated to 0.45 based on single-track experimental results for Gaussian and ring-shaped laser beams.

3. Results and Discussion

Fig. 3a shows the optimized beam shape. The intensity distribution generated by the LCOS-SLM is shown in Fig. 3b. The measurement was realized using a camera-based beam profiler (FBP-2KF, CINOGY Technologies GmbH, Duderstadt, Germany). Differences between the experimentally realized beam shape and the optimized beam shape result both from the IFTA result due to a certain inaccuracy of the approximation and from deviations of the LCOS-SLM from the ideal behavior. The optimized beam shape results in an integrated laser power of 473 W for the calculated beam shape. For the experimental validation, the values were rounded and the parameter set of a laser power P_{laser} of 500 W and a scanning speed v_{scan} of 700 mm/s was defined as reference point. Surrounding this parameter set, the laser power was varied in 4 steps and the scanning speed in 2 steps to investigate the robustness of the calculated beam shape when not using the initially assumed process parameters. All experimentally investigated process parameters are listed in Table 3. For each parameter set, three single tracks were prepared and analyzed.

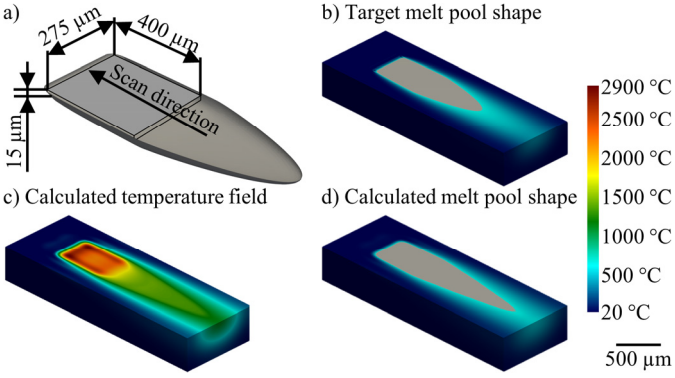

Fig. 2. Temperature fields related to beam shape optimization: (a) target melt pool shape, (b) temperature field for target melt pool shape, (c) calculated output temperature field from optimization algorithm, (d) calculated melt pool shape from optimization algorithm.

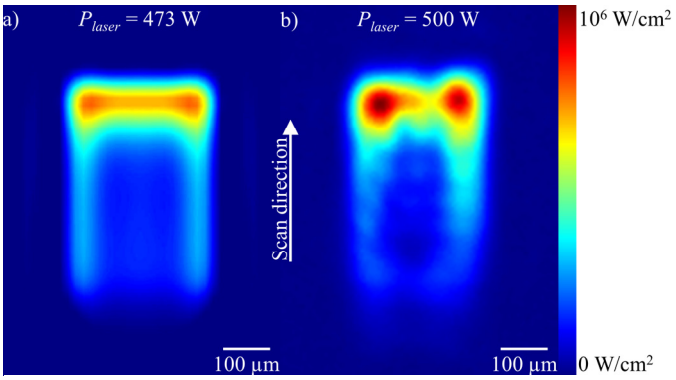

Fig. 3. (a) Optimized calculated; (b) experimentally generated beam shape.

Fig. 4 compares the calculated melt pool cross-section (see Fig. 4a to the experimentally generated melt pool cross-section (see Fig. 4b. The experimentally generated cross-section is slightly broader than the calculated one. This is assumed to relate to the higher intensities in the front area of the beam shape (see Fig. 3). In addition, it can be seen that the melt pool in the experiment is beginning to bulge slightly in the center. These fluid mechanical effects are neglected in the simulation. For this reason, respective effects cannot be observed in the calculated melt pool cross-section. However, overall, the dimensions of the simulation and the experiment differ by a maximum of 7 % in the designed parameter set.

Fig. 5 and Fig. 6 show the evaluated weld penetration depths and melt track widths generated with the optimized beam shape. When the process parameters change, the weld penetration depth deviates quite sensitively from the target. With a power deviation of 20 %, the welding depth changes by more than 30 % (see Fig. 5). A deviation in the scanning speed has a relatively uniform effect. If the scanning speed is adjusted by 30 %, the welding depth changes by 30 %. For larger deviations, this scaling is not linear. The melt track width is less sensitive to changes in the process parameters. Across all parameter sets investigated, the fusion track widths deviate by a maximum of 15 % from the target width, although the applied power differs by up to 40 % (see Fig. 6). This is because the melt track width depends less on the power or energy applied than the spot size perpendicular to the scan direction and the time available for heat conduction [17]. This time depends on the spot size in the scanning direction and the scanning speed [17]. As in the present study the spot size is large, the influence of the varied process parameters is comparatively low.

According to the approaches of Hann et al. [18], the weld penetration depth can be correlated well with the dimensionless enthalpy. The approach also works for non-Gaussian beam profiles [19]. The essential part of the dimensionless enthalpy that changes in this study is the factor $P_{laser}/v_{scan}^{0.5}$ [20]. The remaining parameters of the dimensionless enthalpy according

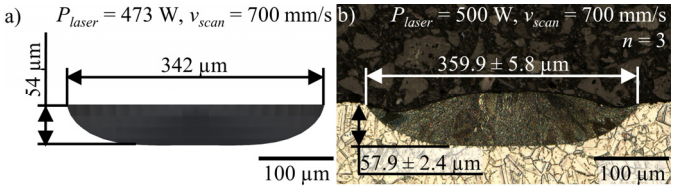

Fig. 4. Comparison of (a) calculated melt pool shape and (b) experimentally generated melt pool shape.

Table 3: Process parameters.

Laser power P_{laser} in W	300, 400, 500, 600, 700
Scan speed v_{scan} in mm/s	500, 700, 900

to [18] remain constant. Therefore, Fig. 7 shows the welding depth as a function of $P_{laser}/v_{scan}^{0.5}$. The weld penetration depth correlates nearly linearly with the varying part of the dimensionless enthalpy. This linear relationship also helps to explain why varying the scanning speed has a smaller influence on the welding depth than changing the laser power.

In addition to the non-uniform behavior of the melting track width and the weld penetration depth, the qualitative shape of the melt pool cross-section also changes. Fig. 8 shows the micrographs of the optimized and surrounding parameter sets. If the laser power is reduced and/or the scanning speed is increased (i.e., $P_{laser}/v_{scan}^{0.5}$ is reduced), the melt pool in the center is no longer as deep as at the edge of the cross-section. The lower edge of the melt pool cross-section is then no longer straight but curves slightly upwards. When the laser power increases and/or the scanning speed is reduced (i.e., $P_{laser}/v_{scan}^{0.5}$ increases), the melt pool cross-section is deeper in the center. In this way, the originally rectangular melt pool cross-section transforms into a semi-circular shape. If the changes in laser power and scanning speed are balanced to keep $P_{laser}/v_{scan}^{0.5}$ in a similar range, the melt pool dimensions and the cross-sectional shape remain almost constant (see black dotted squares in Fig. 7 and Fig. 8. However, as the scanning speed increases, the melt pool increasingly protrudes. This behavior may result in humping or balling effects during the final powder bed fusion process. The process would then no longer be reliable. However, it can be deduced from the experiments that the melt pool dimensions and shape depend primarily on the dimensionless enthalpy (or rather $P_{laser}/v_{scan}^{0.5}$) and cannot be assigned to one single process parameter. With an increased scanning speed of 900 mm/s, the process looks stable on a single-track basis. Therefore, the scanning speed could potentially be increased, and the beam profile could be optimized for the increased scanning speed.

Due to the resulting wide and uniform melt pool shape, the hatch distance may be chosen to be larger compared to the state of the art. Consequently, the build rate $\dot{V}$ can be increased in theory. To quantify the possible increase, a parameter set

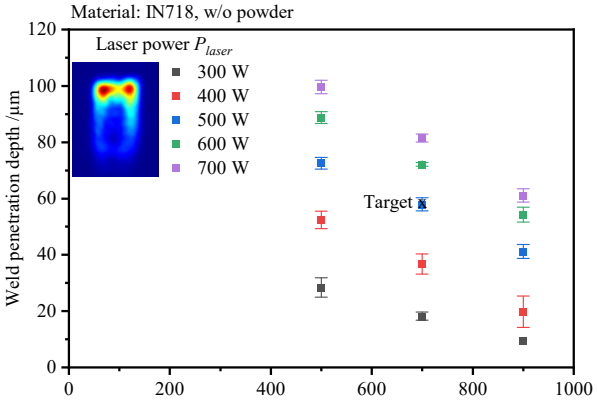

Fig. 5. Weld penetration depth as a function of the scan speed and laser power of the single tracks created with the optimized beam shape.

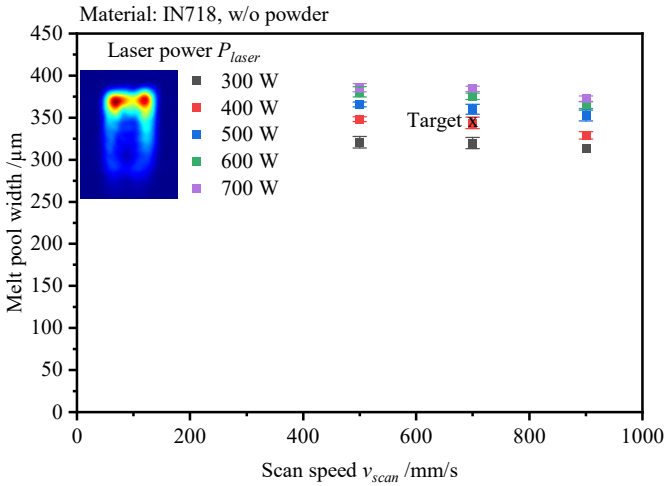

Fig. 6. Melt pool width as a function of the scan speed and laser power of the single tracks created with the optimized beam shape.

frequently used in the literature [2] is used as a reference (see Table 4. With the initial scanning speed of 700 mm/s, the productivity, according to equation 1, can be almost doubled. By increasing the scanning speed to 900 mm/s, an increase in productivity of nearly 150 % would be possible. For a final statement regarding the stability of the PBF-LB/M process with the calculated beam profile, investigations of multi-track and multi-layer specimens are necessary. This is because the presence of powder is likely to increase the balling tendency and enable effects such as powder denudation, making the process more complex than in the shown simplistic validation.

4. Conclusion

This publication explores how to generate brick-like melt pool cross-sections for a PBF-LB/M process. For this purpose, a beam shape is inversely calculated from an approximated temperature distribution corresponding to a brick-shaped melt pool using a numerical optimization framework. The optimized laser beam shape is reproduced, and the melt pool result is validated experimentally on a bead-on-plate single-track basis. In addition, a process parameter space around the initial parameter set is investigated with the optimized beam shape to estimate the robustness of the beam shape in the PBF-LB/M process. The key findings can be summarized as follows:

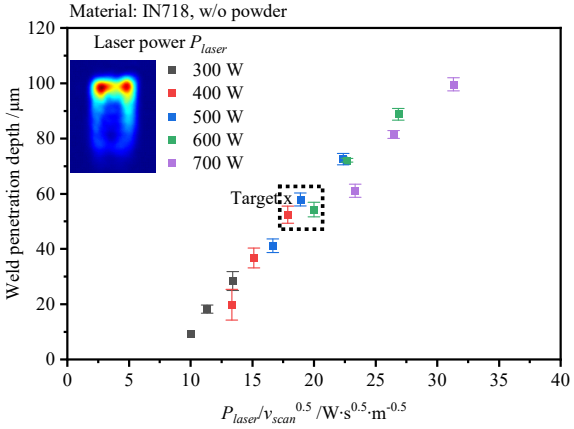

Fig. 7. Weld penetration depth as a function of $P_{laser}/v_{scan}^{0.5}$ of the single tracks created with the optimized beam shape.

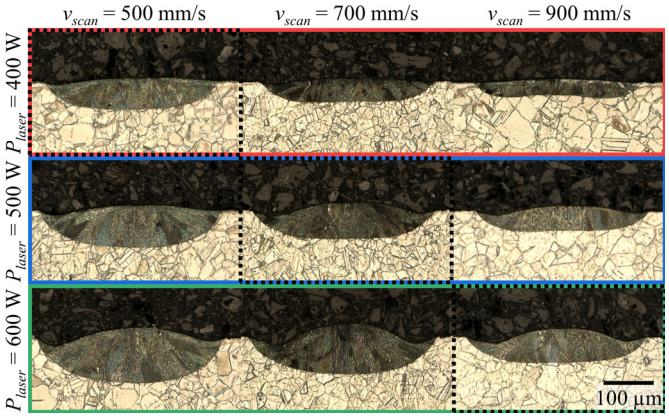

Fig. 8. Micrographs generated with varying laser power and scanning speed.

- Applying an optimization framework enables the inverse calculation of a beam shape, resulting in a desired temperature distribution in PBF-LB/M.
- Using reflective spatial light phase modulators, the calculated beam shape can be approximated experimentally.
- The simulation and the experiments are in excellent agreement. The deviations of the weld penetration depth and melt track width are between 5 % and 7 %.
- The melt pool cross-section depends on the dimensionless enthalpy. Deviations of the dimensionless enthalpy proportionally relate to the weld penetration depth.
- The modified melt pool shape is expected to result in increased productivity by 100 % to 150 %.

Further experiments will show whether the demonstrated potential can be transferred to the final PBF-LB/M process.

Acknowledgments

The European Commission funded the research shown as part of the HORIZON program (Project 101058523 InShaPe). The authors are grateful for the financial funding. Furthermore, the authors acknowledge the funding received by the German Research Foundation (DFG, Deutsche Forschungsgemeinschaft)–grant KO 4570/2-1. Additionally, the authors want to thank the project partner EOS for providing the system technology for the experiments.

References

[1] Khorasani, A., Gibson, I., Veetil, J.K., Ghasemi, A.H., 2020. A review of technological improvements in laser-based powder bed fusion of metal printers. Int J Adv Manuf Technol *108*, p. 191.
[2] Panzer, H., Diller, J., Ehrenfels, F., Brandt, J., Zäh, M.F., 2024. Experimental investigation of process parameter variations on the microstructure and failure behavior of IN718 structures in PBF-LB/M. Journal of Laser Applications *36*.
[3] Li, R., Liu, J., Shi, Y., Wang, L., Jiang, W., 2012. Balling behavior of stainless steel and nickel powder during selective laser melting process. Int J Adv Manuf Technol *59*, p. 1025.
[4] Zöller, C., Adams, N.A., Adami, S., 2023. Numerical investigation of balling defects in laser-based powder bed fusion of metals with Inconel 718. Additive Manufacturing *73*, p. 103658.

Table 4: Comparison of process parameters.

	Reference Gauss	Recommendation (optimized)
Laser power P_{laser}	285 W	500 W
Scan speed v_{scan}	960 mm/s	700 mm/s
Hatch distance h	110 µm	290 µm (expected)
Powder layer thickness t_{powder}	40 µm	40 µm
Build rate $\dot{V}$	4.22	8.12

[5] Galbusera, F., Caprio, L., Previtali, B., Demir, A.G., 2023. The influence of novel beam shapes on melt pool shape and mechanical properties of LPBF produced Al-alloy. Journal of Manufacturing Processes *85*, p. 1024.
[6] Nahr, F., Bartels, D., Rothfelder, R., Schmidt, M., 2023. Influence of Novel Beam Shapes on Laser-Based Processing of High-Strength Aluminium Alloys on the Basis of EN AW-5083 Single Weld Tracks. JMMP *7*, p. 93.
[7] Wischeropp, T.M., Tarhini, H., Emmelmann, C., 2020. Influence of laser beam profile on the selective laser melting process of AlSi10Mg. Journal of Laser Applications *32*.
[8] Grünewald, J., Gehringer, F., Schmöller, M., Wudy, K., 2021. Influence of Ring-Shaped Beam Profiles on Process Stability and Productivity in Laser-Based Powder Bed Fusion of AISI 316L. Metals *11*, p. 1989.
[9] Okunkova, A.A., Peretyagin, P., Podrabinnik, P.A., Zhirnov, I.V., Gusarov, A.V., 2017. Development of Laser Beam Modulation Assets for the Process Productivity Improvement of Selective Laser Melting. Procedia IUTAM *23*, p. 177.
[10] Zhirnov, I.V., Podrabinnik, P.A., Okunkova, A.A., Gusarov, A.V., 2015. Laser beam profiling: experimental study of its influence on single-track formation by selective laser melting. Mechanics & Industry *16*, p. 709.
[11] Cloots, M., Uggowitzer, P.J., Wegener, K., 2016. Investigations on the microstructure and crack formation of IN738LC samples processed by selective laser melting using Gaussian and doughnut profiles. Materials & Design *89*, p. 770.
[12] Mi, Y., Mahade, S., Sikström, F., Choquet, I. *et al.*, 2022. Conduction mode laser welding with beam shaping using a deformable mirror. Optics & Laser Technology *148*, p. 107718.
[13] Rasch, M., Roider, C., Kohl, S., Strauß, J. *et al.*, 2019. Shaped laser beam profiles for heat conduction welding of aluminium-copper alloys. Optics and Lasers in Engineering *115*, p. 179.
[14] Slodczyk, M., Ilin, A., Kiedrowski, T., Schmiemann, J., Ploshikhin, V., 2021. Simulation Aided Process Development with Multi-Spot Strategies in Laser Powder-Bed Fusion. AMR *1161*, p. 75.
[15] Agazhanov, A.S., Samoshkin, D.A., Kozlovskii, Y.M., 2019. Thermophysical properties of Inconel 718 alloy. J. Phys.: Conf. Ser. *1382*, p. 12175.
[16] Holla, V., Kopp, P., Grünewald, J., Wudy, K., Kollmannsberger, S., 2023. Laser beam shape optimization in powder bed fusion of metals. Additive Manufacturing *72*, p. 103609.
[17] Rubenchik, A.M., King, W.E., Wu, S.S., 2018. Scaling laws for the additive manufacturing. Journal of Materials Processing Technology *257*, p. 234.
[18] Hann, D.B., Iammi, J., Folkes, J., 2011. A simple methodology for predicting laser-weld properties from material and laser parameters. J. Phys. D: Appl. Phys. *44*, p. 445401.
[19] Grünewald, J., Wittemer, M., Wudy, K., 2024. Novel Insights in Normalized Process Parameters for Ring-Shaped Beam Profiles in Laser-Based Powder Bed Fusion of Metals. Available at SSRN: http://dx.doi.org/10.2139/ssrn.4744613.
[20] Chechik, L., Schwarzkopf, K., Rothfelder, R., Grünewald, J., Schmidt, M., 2024. Material dependent influence of ring/spot beam profiles in laser powder bed fusion. Additive Manufacturing Letters *9*, p. 100211.